ADVANCED FUNCTIONAL MATERIALS
www.afm-journal.de

Color-Stable, All-Phosphorescent White Organic Light Emitting Diodes Using the Polariton-Enhanced Purcell Effect

*Claire E. Arneson, Haonan Zhao, and Stephen R. Forrest**

The short operational lifetimes of high efficiency phosphorescent organic blue light emitting devices (PHOLEDs) has limited their use in displays and lighting. Previously, this problem has been avoided by using less efficient fluorescent blue devices in separately biased red, green, and blue emissive elements to achieve stable full color emission. However, the operational lifetime of blue phosphorescent OLEDs has been significantly improved through the utilization of the plasmon-exciton-polariton-enhanced (PEP) Purcell effect. Here, a white emitting PHOLED comprising stacked red, green, and blue elements is demonstrated that exploits PEPs to extend the operational lifetime of the blue element such that all emissive layers degrade at the same rate. The device features white light emission with an external quantum efficiency of 19.1 ± 0.4%, luminous power efficiency of 13.3 ± 0.3 lm W^{-1} at a luminance of 1000 cd m^{-2} when measured over 4π solid angle, with a color rendering index of 76 unchanged throughout the device aging to 70% of its initial luminance, T_{70}. A 2.9 times enhancement in the operational lifetime of the Purcell-enhanced device is achieved to yield T_{70} = 2900 ± 100 h for an initial luminance of 1000 cd m^{-2}, compared to devices lacking this enhancement with T_{70} = 1000 ± 100 h.

1. Introduction

Many attributes of phosphorescent organic light emitting diodes (PHOLEDs), such as a high internal quantum efficiency, wide color gamut, and accurate color rendering are desirable for both display and lighting applications.[1–3] Because white light is generated by exciting a combination of red, green, and blue emitting molecules, it is necessary for the lifetime of each element to be stable and importantly, comparable such that the color quality of the device does not noticeably change over its lifetime. Currently, both phosphorescent and fluorescent red and green OLEDs at L = 1000 cd m^{-2} can achieve commercially acceptable operational lifetimes of >180 000 h before reaching 70% of their initial luminance (T_{70}).[3] However, the lifetimes of blue phosphorescent emitters have lagged relative to their lower energy emitting red and green analogs, with light blue emitters demonstrating commercial operational lifetimes of 20 000 when aged at 1 000 cd m^{-2} to T_{50}.[3,4] Previous studies have shown blue PHOLED lifetimes are limited by the generation of high energy excited states produced by triplet-triplet and triplet-polaron annihilation. These states have energies greater than the bond dissociation energies within the molecules, thus leading to molecular fragmentation.[5,6] For this reason, improved stability is achieved using less efficient fluorescent blue coupled with phosphorescent red and green emitters in white OLEDs (WOLEDs).[7–12] To achieve all-phosphorescent WOLEDs it is necessary to compensate for the short blue emitter lifetime through the choice of materials and emission layer (EML) design, such as graded doping or hot excited state management.[13,14] Despite achieving high efficiencies while maintaining a high color rendering index (CRI), to our knowledge a color-stable all phosphorescent WOLED has not yet been reported.[15–21] Recently, Zhao, et al. demonstrated the improvement of blue PHOLED operational lifetimes by more than a factor of four compared to conventional devices through the plasmon-exction-polariton (PEP)-enhanced Purcell effect. Here, PEPs result in an increase in the Purcell factor and improved coupling of energy from the EML to plasmonic modes on the metal cathode; both of which contribute to an enhancement in device lifetime.[22]

The Purcell factor (PF) is defined as the cavity-enhanced triplet emission rate via $k_r = PF \cdot k_{r0}$, where k_{r0} is the natural triplet

C. E. Arneson, H. Zhao, S. R. Forrest
Department of Physics
University of Michigan
Ann Arbor, MI 48109, USA
E-mail: stevefor@umich.edu, forrest@princeton.edu
S. R. Forrest
Applied Physics Program
University of Michigan
Ann Arbor, MI 48109, USA
S. R. Forrest
Department of Electrical Engineering and Computer Science
University of Michigan
Ann Arbor, MI 48109, USA
S. R. Forrest
Department of Materials Science and Engineering
University of Michigan
Ann Arbor, MI 48109, USA

The ORCID identification number(s) for the author(s) of this article can be found under https://doi.org/10.1002/adfm.202410741

© 2024 The Author(s). Advanced Functional Materials published by Wiley-VCH GmbH. This is an open access article under the terms of the Creative Commons Attribution-NonCommercial-NoDerivs License, which permits use and distribution in any medium, provided the original work is properly cited, the use is non-commercial and no modifications or adaptations are made.

DOI: 10.1002/adfm.202410741

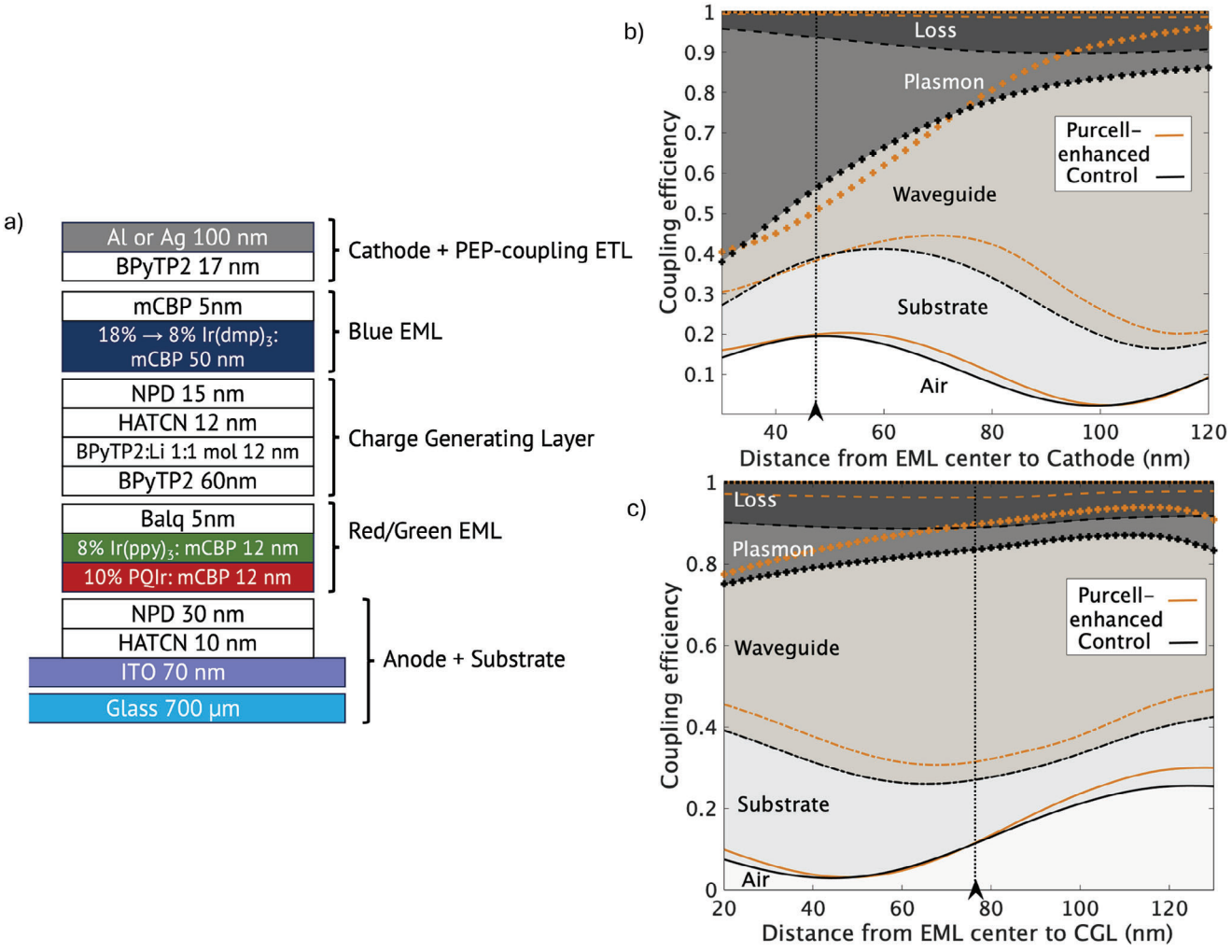


Figure 1. a) Schematic illustration of the device structure. Coupling efficiencies to lossy, surface plasmon polariton, organic waveguide, substrate, and air modes are calculated using Green's function methods for the blue, b), and red/green, c), elements. The control devices are indicated by the shaded areas and black lines, and Purcell-enhanced structures are indicated by the orange lines. The horizontal axis shows the results for various spacings between the blue EML and the cathode, b), and the red/green EML and the CGL, c). The dotted vertical lines correspond to the structures used in this work. The vertical axis shows the fractional coupling efficiency into each mode, where the total of all modes is equal to 1. The fraction of coupling to each mode can be found by the vertical distance between black lines for the control, and orange lines for the Purcell-enhanced structure.

radiative rate. This phenomenon, known as the Purcell effect, is used to increase the radiative optical density of states within the PHOLED, thereby reducing the radiative lifetime of triplets. This, in turn, reduces their density within the EML, and thus the probability to produce high energy and damaging hot excited states. The Purcell effect is amplified by energy transfer to PEP modes formed at the interface between the electron-transporting layer (ETL) and the cathode. Coupling of plasmons in the Ag cathode adjacent to polaritons in the ETL significantly strengthens the Purcell effect compared to conventional PHOLEDs with an Al cathode. Previously, we demonstrated that the blue emissive element in a side-by-side WOLED degrades ≈2.5 times faster to T_{70} than the red/green pixel operated at the same current density.[23] This suggests that the PEP-enhanced Purcell effect can stabilize the blue emission to the point where its lifetime is comparable to the red and green elements.

Here, we demonstrate an all-phosphorescent stacked WOLED comprising a blue element adjacent to the cathode that is connected via a charge generation layer to a red/green emitting element, shown in **Figure 1**a. We compare conventional devices employing an Al cathode (the control), to devices in which the radiative lifetime of the blue element is modified by PEPs through use of a Ag cathode (the Purcell-enhanced device) and an exciton-polariton coupling layer of BPyTP2. The BPyTP2 singlet emission spectrum overlaps the Ag plasmon absorption, and its absorption spectrum overlaps with the blue emission from the EML. The resulting strongly-coupled polariton serves to decrease the triplet density in the EML by enhancing energy transfer from the EML to Ag plasmon modes. We achieved an initial external quantum efficiency of $EQE_{4\pi}$ = 19.1 ± 0.4% measured at 4π sr with a CRI = 76 and a correlated color temperature of CCT = 6100 K for the Purcell-enhanced device. This is compared with $EQE_{4\pi}$ = 13.0 ± 0.4% with CRI = 74 at 6900K for the control. We

© 2024 The Author(s). Advanced Functional Materials published by Wiley-VCH GmbH

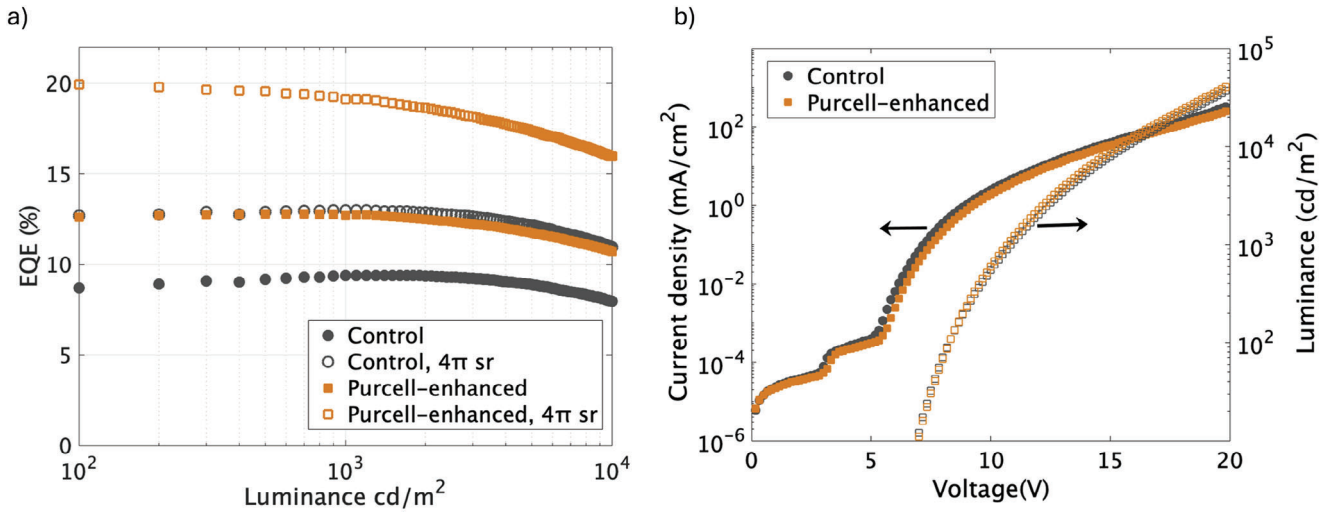


Figure 2. a) Device external quantum efficiency for forward viewing in 2π solid angle (filled symbols) and 4π solid angle with an external microlens array (open symbols) as a function of brightness. b) Current–voltage–luminance characteristics of the control and Purcell-enhanced devices.

observe no measurable change in the colorimetric values for both devices at T_{70}, maintaining 1960 Commission Internationale de l'Eclairage (CIE) coordinates (u,v) = (0.17, 0.32) for the control and (0.18, 0.33) for the Purcell-enhanced devices. These latter WOLEDs exhibit an extrapolated T_{70} = 2900 ± 100 h at an initial luminance of 1000 cd m^{-2}, which is a 2.9 times improvement over the control device lifetime, as predicted by simulations.[22] By using the PEP-enhanced Purcell effect, we demonstrate a WOLED with CRI >75 that shows a significant improvement in the color stability during aging when compared to previously reported WOLEDs, summarized in Table S1 (Supporting Information).

2. Results

The stacked WOLED in Figure 1a comprises two emissive layers, one red/green (R/G) and the other blue (B), separated by a charge generation layer (CGL). The control structure employs an Al, cathode, and the other a Purcell-enhanced, Ag, cathode. In both structures, BPyTP2 is used as the ETL. See Methods for IUPAC nomenclature for materials used. Overlap between the blue triplet and the BPyTP2 singlet exciton absorption spectra in Figure S1 (Supporting Information), and the BPyTP2 emission and the Ag plasmon mode absorption enables efficient energy transfer to PEPs, as shown previously.[22] This is not observed in the control, where Al has only a weak plasmon resonance in the blue.

The coupling efficiencies into various available WOLED modes for photons emitted from the B and R/G elements calculated using Green's function methods are shown in Figure 1b,c, respectively.[24] The distances of the B EML to the cathode, and the R/G EML to the CGL used in optimized devices are shown by dashed vertical lines. The calculated weighted average PF = 0.95 and 1.7 for the R/G and B layers within the control device, respectively, are compared with 0.91 and 2.2, respectively in the Purcell-enhanced device. Details on the calculation of the PF are included in Methods. The PF average, which depends on the

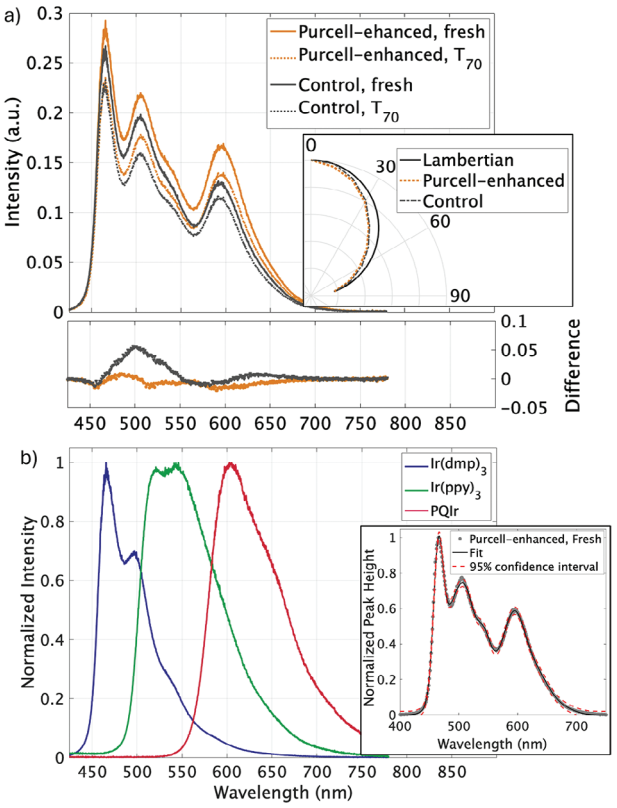


Figure 3. a) Device spectra measured at normal incidence for both control and Purcell-enhanced devices before aging (fresh) and at T_{70}. The differences between normalized spectra for control and Purcell-enhanced devices are indicated on the right axis of the lower plot. *Inset*: Angular device emission profile. A Lambertian profile is indicated by the black line for reference. b) Individual spectra for Ir(dmp)$_3$ (blue), Ir(ppy)$_3$ (green), and PQIr (red) phosphors in thin films. *Inset*: Fitting using the individual spectra for the fresh, white-emitting Purcell-enhanced device.

© 2024 The Author(s). Advanced Functional Materials published by Wiley-VCH GmbH

Table 1. As-prepared Device Colorimetric Parameters.

	1960 CIE (u, v)	CRI	CCT (K)	Δuv
Control	(0.17, 0.32)	74	6900	0.031
Purcell-enhanced	(0.18, 0.33)	76	6100	0.025

position in the EML and the exciton concentration at each EML position, is weighted by the distribution of dopants throughout the EML. That is, dopant emission closer to the cathode has a higher PF than emission near the hole transport layer/EML interface. From Figure 1b,c, there is a negligible change in the peak outcoupling efficiency between the control and Purcell-enhanced structures, from 16% to 17% for R/G, and no change for B. Coupling to plasmon modes is increased from 37% to 48% for B in the control and Purcell-enhanced devices, respectively.

The external quantum efficiencies in the forward viewing and 4π viewing directions are shown in **Figure 2a**. We approximate the operating conditions of a white lighting fixture by accounting for emission from 4π sr and adding an external microlens array. Under these conditions, $EQE_{4\pi} = 12.8 \pm 0.1\%$ and $19.1 \pm 0.3\%$, and $LPE_{4\pi} = 7.8 \pm 0.1$ and 10.8 ± 0.2 lm W^{-1} for control and Purcell-enhanced devices, respectively, corresponding to $L = 3300 \pm 20$ and 4330 ± 60 cd m^{-2} at $J = 10$ mA/cm^2.

The L–V characteristics of the control and Purcell-enhanced devices are nearly identical, as shown in Figure 2b. Similarly, there are no significant changes in the J–V characteristics between devices employing an Ag or Al cathode, whose turn on voltages are ≈5.3 V. This is nearly double the voltage observed for single junction devices, since the B subelement, with a turn-on of 3 V, and R/G, with a turn-on of 2.5 V, are connected in series.[23]

The emission spectra and spatial emission profiles both before and after aging at $J = 10$ mA cm^{-2}, are shown in **Figure 3a**. The control and Purcell-enhanced devices cover 92% and 94% of the Lambertian profile, respectively, resulting in a shift in 1960 CIE (u, v) chromaticity coordinates of $(\Delta u, \Delta v) = (0.04, 0.01)$ between viewing angles of 0° and 80°, as the effective cavity length decreases with increasing viewing angle.[25] The colorimetric coordinates, CRI, CCT, and the distances from the Planckian locus (Δuv) for the devices are provided in **Table 1**.

The devices were aged at $J = 10$ mA cm^2, with results shown in **Figure 4**. We obtain the times to reach 70% of their initial luminance of $T_{70} = 1030 \pm 20$ and 2900 ± 100 h, with a corresponding increase in voltage at a constant J of $\Delta V = 1.36 \pm 0.03$ and 1. 13 ± 0.01 V for the control and Purcell-enhanced devices, respectively.

At T_{70} there is no measurable change in device (u, v) chromaticity coordinates and CRI for either device, although the control electroluminescence spectrum exhibits a small change in wavelength dependence with aging corresponding to a red shift in CCT, $\Delta CCT = 100$K, while there is no measurable wavelength or CCT shift for the Purcell-enhanced device (see Figure 3a). The wavelength changes are characterized by fitting the white spectrum to the sum of the individual spectra of the separate red, green, and blue emitting materials provided in Figure 3b, corresponding to three peaks from Ir(dmp)$_3$ and Ir(ppy)$_3$, and two from PQIr. A representative fit for the Purcell enhanced device is shown inset of Figure 3b, with a summary of all fit parameters found in **Table 2**. Using these fits, we determine the change in spectra from their differences also shown in Figure 3b. The Purcell-enhanced devices show a nearly uniform <6% change in peak magnitude across all wavelengths, while the control exhibits a 47% decrease in the 524 nm vibronic of Ir(dmp)$_3$, and a >8% change across red and green.

The lifetime is normalized to an initial luminance of $L_0 = 1000$ cd m^{-2} using:[3]

$$T_X\ (L_0) = T_X\ (L_{0,test})\ (L_{0,test}/L_0)^n \quad (1)$$

where T_X is the device lifetime at a fraction, x, of the initial luminance. The acceleration factor, $n = 1.3 \pm 0.1$ for the control and $n = 1.5 \pm 0.1$ for the Purcell-enhanced device is found by solving Equation (1) using the lifetime and initial luminance of devices aged at $J = 5$ and $J = 10$ mA cm^{-2}, with data compiled in **Table 3**. We find that for $L_0 = 1000$ cd m^{-2}, the operational lifetime is $T_{70} = 1030 \pm 40$ h for the control and 2900 ± 60 h for the Purcell-enhanced devices, demonstrating a 2.9 times enhancement. Raw data for devices aged at equivalent current densities before normalizing to constant luminance are shown in Figure S2 (Supporting Information).

3. Discussion

The device stack in Figure 1a employs a 17 nm thick BPyTP2 ETL to optimize coupling between the blue EML and plasmonic modes formed on the metal cathode surface and outcoupling to air modes of emission from both the B and R/G EMLs. A thinner ETL suppresses outcoupling to air modes as shown in Figure 1b, while a thicker ETL decreases coupling to the SPP modes formed at the control ETL/Al interface and PEP modes at the ETL/Ag interface.[22] The outcoupling efficiency of the R/G element is optimized for a 100 nm thick ETL; in this work, we use a thickness of 60 nm, which is sufficient to provide outcoupling efficiencies of ≈17% for both the Purcell-enhanced and control devices, with 20% for the blue element, and is sufficiently thin to assure a low operating voltage. Additional fresh data for a device with an 80 nm thick R/G ETL is shown in Table S2 and Figure S3

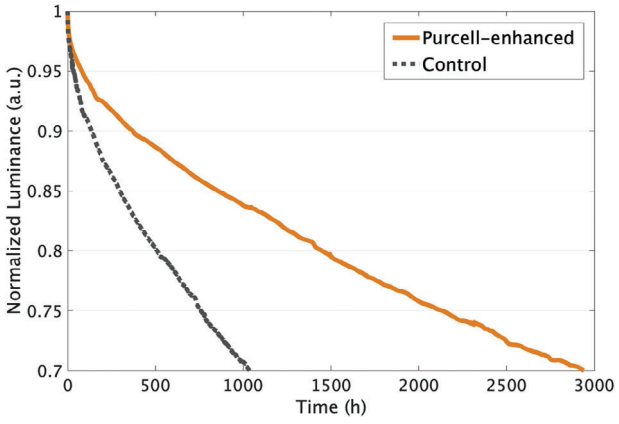


Figure 4. Change in luminance versus time for control and Purcell-enhanced devices, normalized to aging at an initial luminance of 1000 cd m^{-2}.

© 2024 The Author(s). Advanced Functional Materials published by Wiley-VCH GmbH

Table 2. Spectral Parameters.

		Normalized Peak Height					
		Purcell-enhanced			Control		
		Fresh	T_{70}	Δ%*	Fresh	T_{70}	Δ%
	R-sqared value	0.9988	0.9987		0.9982	0.9979	
	RMS Error	0.01	0.01		0.01	0.01	
Dopant	Center wavelength (nm)						
Ir(dmp)3	465	0.73	0.72	-1.2	0.70	0.70	-1.2
	491	0.55	0.55	-1.2	0.54	0.53	-1.2
	524	0.25	0.24	-5.4	0.20	0.10	-47.5
Ir(ppy)3	513	0.16	0.17	5.9	0.16	0.19	17.9
	543	0.21	0.22	5.9	0.21	0.25	17.9
	584	0.32	0.32	1.4	0.29	0.31	8.5
PQIr	631	0.21	0.22	3.4	0.17	0.15	-10.9
	596	0.23	0.24	3.4	0.18	0.16	-10.9

*Δ% is defined as the percent change in peak intensity from the fresh to T_{70} fit.

(Supporting Information), which demonstrates a red shift in its spectrum because of the increased ETL thickness. The redshift is the result of higher coupling to air modes from the R/G layer, shown in Figure 1c. However, there is no significant difference in the electrical performance between 60 and 80 nm ETL devices, indicating the charge balance is better for the device with the thinner ETL. The cathode/ETL structure is optimized for the B element. Because R/G emission is generated far from the cathode, the dependence of R/G outcoupling on B ETL thickness, shown in Figure S4 (Supporting Information), varies by only ≈7% across a 15 nm range of B ETL thicknesses, which is less than half the observed change in plasmon coupling for emission from the B EML across the same range. Thus, the choice of B ETL thickness can be optimized independently of the R/G subelement. In the blue EML, the Purcell-enhanced structure increases *PF* by a factor of 1.4 relative to the control.

The CGL between the B and R/G elements enables each injected electron to generate two photons. The measured forward direction EQE = 12.2%, therefore, is low due to the relatively low quantum efficiencies of both the B and R/G emitting sections. That is, the discrete blue-emitting $Ir(dmp)_3$ devices have EQE = 9.5%, and R/G devices have EQE = 12%.[13,23] Indeed, conventional WOLEDs used in lighting have up to 5 or 6 emitting sections to achieve high efficiency and brightness. Nevertheless, this relatively simple archetype device achieves CRI = 76 at a high color temperature of CCT = 6100 due to strong blue emission, that is unchanged over the course of aging. The chromaticity coordinates have a minimal viewing angle dependence, showing a slight blue shift from a viewing angle of 0° to 80°. The corresponding change in the distance from the u,v coordinates to the closest point on the Planckian locus, Δuv, shifts $\delta\Delta uv = -0.033$ for the control and -0.035 for the Purcell-enhanced devices, where $\delta\Delta uv$ is defined as the change in Δuv.[23]

The stability of the blue emission is due to the reduced radiative lifetime resulting from coupling between the triplets and SPP modes in the control device. In comparison, previously demonstrated long-lived stacked WOLEDs have shown noticeable redshifts at T_{70}, corresponding to a 50% decrease in luminance from the blue despite the use of triplet managers to extend the blue emitter lifetime.[18] In work that utilizes the same EML structures in a side-by-side rather than stacked geometry, a red shift of $(\Delta u,\Delta v) = (0.014,-0.002)$ is observed, while here $(\Delta u,\Delta v) = (0.002, 0.000)$ falls within the margin of error.[23] This demonstrates a significant improvement over previous WOLEDs with both phosphorescent and fluorescent blue emitters where $(\Delta u,\Delta v)$ is 10 × greater, or color stability has not been reported.[10–12,15–21,26–29] A summary of reported WOLED data in the literature is included in Table S1 (Supporting Information). In the Purcell-enhanced device, blue triplets are strongly coupled to PEP modes, resulting in improved spectral stability (cf. Figure 3a) along with a significant increase in lifetime. Use of the PEP-enhanced Purcell effect results in a reduction in the voltage rise over the course of aging by 0.23 V compared to the control, and a 2.9 times increase in T_{70}. This operational lifetime

Table 3. Lifetime and Aging Parameters.

	5 mA cm^{-2}			10 mA cm^{-2}							
	L_0 (cd m^{-2})	L_0 *) (cd m^{-2})	T_{90} (h)	L_0 (cd m^{-2})	L_0 *) (cd m^{-2})	T_{90} (h)	T_{70} (h)	PF	n	T_{70} +) (h)	T_{70} +), *) (h)
Control	1120	1550	73	2240	3300	29	219	1.6	1.3	640	1030
Purcell-enhanced	1389	2270	125	2940	4330	41	325	2.2	1.5	1600	2940

*Measured using an external microlens array and integrating sphere; +Normalized to L_0 = 1000 cd m^{-2}.

© 2024 The Author(s). Advanced Functional Materials published by Wiley-VCH GmbH

enhancement is in agreement with the 2.9 times enhancement expected at T_{70} based on the power law, $m = 1.7 \pm 0.1$, dependence between PF and operational lifetime (i.e., $T_x \approx PF^m$), as previously reported.[22]

4. Conclusion

We demonstrated a stacked white-emitting PHOLED with improved operational lifetime due to exciton-plasmon-polariton coupling that increases the optical density of states within the OLED cavity of the blue subelement. This, in turn, decreases the blue triplet lifetime, thereby reducing the probability for generating high energy excited states via triplet annihilation processes that lead to molecular dissociation. We observe no change in emission color across the entire white spectrum for Purcell-enhanced devices, demonstrating that the polariton-enhanced Purcell effect improves B subelement lifetime such that it degrades at the same rate as the R/G subelement. While this work demonstrates a relatively simple device design with a high CRI and operational stability, the color quality and lifetime can be further improved by increasing the strength of the Purcell effect with a sub-anode reflector and increasing EQE using more efficient blue phosphorescent material. Furthermore, high brightness and efficient stacked PHOLEDs typically are comprised of at least 3–5 R/G elements to improve both lifetime and CRI.[18] The design introduced here only affects the blue emitting subelement in the stack near the cathode, and hence does not preclude the addition of more R/G elements to achieve practical long-lived, bright, and color-balanced emission.

5. Experimental Section

Device Fabrication: Prior to organic layer deposition, pre-patterned ITO anodes (15 Ω sq^{-1}) on glass substrates (Lumtec) were sonicated in detergent, deionized water, acetone (x2), isopropanol (165 °C, x2), and dried using pure N_2. The 2 mm^2 device was defined by the 1 mm width of the ITO stripes and the 2 mm width of the shadow mask placed perpendicular to the ITO used for cathode metal patterning.

Vacuum thermal evaporation was used to deposit the organic layers. As shown in Figure 1a, the layers comprise 10 nm thick hexaazatriphenylene hexacarbonitrile (HATCN, Universal Display Corp., UDC), 30 nm thick N,N'-di(1-naphthyl)-N,N'-diphenyl-(1,1′-biphenyl)−4,4′-diamine (NPD, UDC), 12 nm thick 10% vol bis(2-phenylquinolyl-N,$C^{2'}$) acetylacetonate iridium(III) (PQIr, UDC) doped into 4,40-bis(3-methylcarbazol-9-yl)−2,20-biphenyl (mCBP, UDC), 12 nm thick 8% vol tris[2-phenylpyridinato-C^2,N]iridium(III) ($Ir(ppy)_3$, Lumtec) doped into mCBP, 5 nm thick Bis(8-hydroxy-2-methylquinoline)-(4-phenylphenoxy)aluminum (BAlq, Universal Display Corp.), 10 nm thick 10% vol PQIr:mCBP, 60 nm thick 2,7-bis(2,20-bipyridine-5-yl)triphenylene (BPyTP2, Lumtec), 12 nm thick 1:1 mol BPyTP2:Li (Kurt J. Lesker), 12 nm thick HATCN, 15 nm thick NPD, 50 nm thick 18 to 8% vol tris[3-(2,6-dimethylphenyl)−7-methylimidazo[1,2-f] phenanthridine] iridium(III) ($Ir(dmp)_3$:mCBP, UDC), 5 nm thick mCBP, 17 nm BPyTP2, and 1.5 nm thick Li quinolate (Liq, Lumtec). Control devices have a 100 nm thick Al (Alfa Azar) cathode, and Purcell-enhanced devices have a 120 nm thick Ag (Sigma–Aldrich) cathode. Organic materials from Lumtec are purified via thermal gradient sublimation.[30] The devices are encapsulated in ultrapure N_2 with glass cover slide attached using UV-curing epoxy (Epotek).

Device Modeling, Characterization, Lifetime Testing: The forward, 2π, *J–V–L* characteristics were measured using a parameter analyzer (Keysight) and a large area Si photodetector (Hamamatsu). The 4π measurements use an integrating sphere with a commercial external microlens array (Lumtec). Error reported is the standard deviation from a population of four devices. Electroluminescence and angle-dependent spectra were measured via fiber coupling to a spectrometer (Ocean Optics). Device spectra were fit to Gaussian functions using MATLAB. The devices were aged under constant current, supplied by a source-measuring unit (Agilent), and device luminance was measured at 1–3 min intervals using a photodiode. The coupling efficiencies were calculated using Green's function methods.[24] Following the work of Celebi, et al., the Chance, Prock, and Sibley model was used to describe the electric field of an emissive dipole using dyadic Green's functions in the stacked structure shown in Figure 1a. The layer thicknesses and complex indexes of refraction were measured by ellipsometry (J.A. Woollam). From the model, the ratio of the decay rate for vertical and horizontal dipoles, $b_{||}$ and $b_{\perp}$, to the natural decay rate, b_0, in vacuum was computed:

$$\frac{b_{||}}{b_0} = 1 - q + q\left\{1 + \frac{3}{4}\mathrm{Re}\left[\int_0^{\infty} d\kappa \frac{\kappa}{h_s k_s}\left(c_s + c_s' + \frac{h_s^2}{k_s^2}\left(f_s - f_s'\right)\right)\right]\right\} \quad (2)$$

and

$$\frac{b_{\perp}}{b_0} = 1 - q + q\left\{1 + \frac{3}{2}\mathrm{Re}\left[\int_0^{\infty} d\kappa \frac{\kappa^3}{h_s k_s^3}\left(f_s + f_s'\right)\right]\right\} \quad (3)$$

where q is the quantum yield of the emitter, κ and h are the parallel and perpendicular amplitudes of the propagation vector k, f and c, and f' and c' are left and right travelling wave coefficients of the Green's functions used to describe the dipole source, and the subscript s is the index of the dipole emitting layer. Because the PF is equivalent to the total decay rate, then:

$$PF = b_{tot} = \theta_{hor}\frac{b_{||}}{b_0} + (1 - \theta_{hor})\frac{b_{\perp}}{b_0} \quad (4)$$

where θ_{hor} is the horizontal dipole fraction. PF is calculated with 1 nm resolution throughout the EML, and the average PF is weighted by the doping concentration across each EML. It is assumed that the exciton concentration is proportional to the dopant concentration.[13] We assume $\theta_{hor} = 0.77$ and $q = 0.45$ for the B EML and $q = 0.95$ for the R/G EML. The peak emissive wavelengths of $\lambda = 600$ nm and $\lambda = 475$ nm are used for the R/G and B EML calculations, respectively.

Supporting Information

Supporting Information is available from the Wiley Online Library or from the author.

Acknowledgements

The authors acknowledge Universal Display Corporation and the U.S. Department of Energy's Office of Energy Efficiency and Renewable Energy (EERE) under the Award Number DE-EE0009688. This report was prepared as an account of work sponsored by an agency of the United States Government. Neither the United States Government nor any agency thereof, nor any of their employees, makes any warranty, express or implied, or assumes any legal liability or responsibility for the accuracy, completeness, or usefulness of any information, apparatus, product, or process disclosed, or represents that its use would not infringe privately owned rights. Reference herein to any specific commercial product, process, or service by trade name, trademark, manufacturer, or otherwise does not necessarily constitute or imply its endorsement, recommendation, or favoring by the United States Government or any agency thereof. The views and opinions of authors expressed herein do not necessarily state or reflect those of the United States Government or any agency thereof.

© 2024 The Author(s). Advanced Functional Materials published by Wiley-VCH GmbH

Conflict of Interest

One of the authors (SRF) has an equity interest in Universal Display Corporation (UDC). This conflict of interest in under management by the University of Michigan's Office of the Vice President for Research. The University of Michigan has a license agreement with UDC.

Author Contributions

C.E.A fabricated and measured all devices. C.E.A. and H.Z. designed the devices. C.E.A., H.Z., and S.R.F. analyzed the data, and S.R.F. supervised the project. The manuscript was written by C.E.A. and S.R.F. and edited by all co-authors.

Data Availability Statement

The data that support the findings of this study are available from the corresponding author upon reasonable request.

Keywords

blue phosphorescence, electrophosphorescence, lighting, polariton, Purcell Effect

Received: June 19, 2024
Revised: August 7, 2024
Published online: August 29, 2024

[1] F. So, J. Kido, P. Burrows, *MRS Bull.* **2008**, *33*, 663.
[2] Z. Wu, D. Ma, *Mater. Sci. Eng. R Rep.* **2016**, *107*, 1.
[3] S. R. Forrest, *Organic Electronics: Foundations to Applications*, Oxford University Press, USA, **2020**.
[4] C. Adachi, M. A. Baldo, M. E. Thompson, S. R. Forrest, *J. Appl. Phys.* **2001**, *90*, 5048.
[5] N. C. Giebink, D'B. W. Andrade, M. S. Weaver, P. B. MacKenzie, J. J. Brown, M. E. Thompson, S. R. Forrest, *J. Appl. Phys.* **2008**, *103*, 044509.
[6] C. Jeong, C. Coburn, M. Idris, Y. Li, P. I. Djurovich, M. E. Thompson, S. R. Forrest, *Org. Electron.* **2019**, *64*, 15.
[7] J. Birnstock, G. He, S. Murano, A. Werner, O. Zeika, *SID Symp. Dig. Tech. Pap.* **2008**, *39*, 822.
[8] T. K. Hatwar, J. P. Spindler, M. Kondakova, D. Giesen, J. Deaton, J. R. Vargas, *SID Symp. Dig. Tech. Pap.* **2010**, *41*, 778.
[9] H. Kanno, N. C. Giebink, Y. Sun, S. R. Forrest, *Appl. Phys. Lett.* **2006**, *89*, 023503.
[10] Y. Chen, D. Yang, X. Qiao, Y. Dai, Q. Sun, D. Ma, *J. Mater. Chem. C* **2020**, *8*, 6577.
[11] C. Huang, Y. Zhang, J. Zhou, S. Sun, W. Luo, W. He, J. Wang, X. Shi, M. Fung, *Adv. Opt. Mater.* **2020**, *8*, 2000727.
[12] F. Liu, H. Liu, X. Tang, S. Ren, X. He, J. Li, C. Du, Z. Feng, P. Lu, *Nano Energy* **2020**, *68*, 104325.
[13] Y. Zhang, J. Lee, S. R. Forrest, *Nat. Commun.* **2014**, *5*, 5008.
[14] J. Lee, C. Jeong, T. Batagoda, C. Coburn, M. E. Thompson, S. R. Forrest, *Nat. Commun.* **2017**, *8*, 15566.
[15] S. Reineke, F. Lindner, G. Schwartz, N. Seidler, K. Walzer, B. Lüssem, K. Leo, *Nature* **2009**, *459*, 234.
[16] Q. Ou, L. Zhou, Y. Li, S. Shen, J. Chen, C. Li, Q. Wang, S. Lee, J. Tang, *Adv. Funct. Mater.* **2014**, *24*, 7249.
[17] S. Wu, S. Li, Y. Wang, C. Huang, Q. Sun, J. Liang, L. Liao, M. Fung, *Adv. Funct. Mater.* **2017**, *27*, 1701314.
[18] C. Coburn, C. Jeong, S. R. R. Forrest, *ACS Photonics* **2018**, *5*, 630.
[19] S. Jeon, S. Lee, K. Han, H. Shin, K. Kim, J. Jeong, J. Kim, *Adv. Opt. Mater.* **2018**, *6*, 1701349.
[20] H. Yu, X. Dai, F. Yao, X. Wei, J. Cao, C. Jhun, *Sci. Rep.* **2018**, *8*, 6068.
[21] L. Ameri, L. Cao, X. Tan, J. E. Li, *Adv. Mater.* **2023**, *35*, 2208361.
[22] H. Zhao, C. E. Arneson, D. Fan, S. R. Forrest, *Nature* **2024**, *626*, 300.
[23] C. Arneson, X. Huang, S. R. Forrest, *ACS Photonics* **2023**, *10*, 526.
[24] K. Celebi, T. D. Heidel, M. A. Baldo, *Opt. Express* **2007**, *15*, 1762.
[25] V. Bulović, V. Khalfin, G. Gu, P. Burrows, D. Garbuzov, *Phys. Rev. B – Condens. Matter Mater. Phys.* **1998**, *58*, 3730.
[26] L. Zhu, Y. Zhao, H. Zhang, J. Chen, D. Ma, *J. Appl. Phys.* **2014**, *115*, 244512.
[27] J. Yao, W. Liu, C. Lin, Q. Sun, Y. Dai, X. Qiao, D. Yang, J. Chen, D. Ma, *J. Mater. Chem. C* **2021**, *9*, 3626.
[28] C. Zhang, Y. Lu, Z. Liu, Y. Zhang, X. Wang, D. Zhang, L. Duan, *Adv. Mater.* **2020**, *32*, 2004040.
[29] Z. Wang, X. Li, Z. Ma, X. Cai, C. Cai, S. Su, *Adv. Funct. Mater.* **2018**, *28*, 1706922.
[30] S. R. Forrest, *Chem. Rev.* **1997**, *97*, 1793.

© 2024 The Author(s). Advanced Functional Materials published by Wiley-VCH GmbH